Proceedings of the 16th Asian Congress of Fluid Mechanics
13-17 December 2019, Bengaluru, India

Airflow and Particle Transport to the Terminal Bronchioles during Heliox Breathing

Suvash C. Saha[1*], Mohammad S. Islam[1]

[1]School of Mechanical and Mechatronic Engineering
University of Technology Sydney, Sydney, NSW-2007, Australia

*E-mail of corresponding/presenting author: suvash.saha@uts.edu.au

Abstract

The understanding of the airflow and particle transport to the deeper airways is important for targeted drug transport to the terminal bronchioles. The available literature reports only a small portion of the pharmaceutical drug can reach to the targeted position of the lower airways. This study aims to develop a numerical framework to transport the drug particle to the lower airways of a whole lung model. A digital 17-generation lung model is used to perform the airflow and particle transport study. ANSYS Fluent 19.2 solver is used for the numerical calculations. Discrete phase method and species transport model are used for the particle transport and heliox gas mixture respectively. The numerical result illustrates higher near-wall velocity magnitude for the air-breathing than heliox breathing. The species transport model shows lower deposition at the upper airways than the air breathing. The findings of the present study would improve the understanding of heliox therapy, which potentially improves the targeted drug delivery efficiency to the lower airways.

Keywords Helium-Oxygen, Aerosol Particle, Deposition, Drug Delivery.

1. Introduction

Breathing gas-exchange in obstructive and narrowed airways of the human lung is complex. Different respiratory diseases like asthma, chronic obstructive pulmonary disease (https://lungfoundation.com.au/health-professionals/clinical-resources/copd/copd-the-statistics/) (https://lungfoundation.com.au/health-professionals/clinical-resources/copd/copd-the-statistics/) occur the different morphological change of the lung airways, including reduced lung volume and decrease of the thoracic cavity. The reduced lung volume and narrowed airway occur shortness of breath and chest tightness. The human lung also experiences reduced volume with aging as the airway muscles, and tissues lose their ability to keep the bronchioles open (Skloot, 2017). Acute asthma and COPD patient experience higher airflow resistance within the bifurcating airways (Valli et al., 2007). Helium-oxygen (Heliox) gas mixture has been used for decades to reduce the airflow resistance within the obstructive airways. The heliox gas mixture improves the gas-change efficiency (Valli et al., 2007) and improves the mechanical ventilation of the narrowed airways of acute asthma and bronchiolitis (Kim et al., 2009). Heliox gas mixture is less dense than air, and the lower density of heliox mixture influence the gas-exchange by decreasing the airway resistance (Reuben et al., 2004). The less dense heliox mixture create less turbulent intensity at the larynx and tracheal section of the lung and reduce the pressure gradient at the extra-thoracic region. The use of helium gas for the treatment of acute asthma and obstructive airways is first reported by Barach (Barach, 1935). The use of heliox gas mixture for the treatment of respiratory diseases becomes popular in later 1970s when the death rate of asthma patient rise (Rodrigo et al., 2001). The use of heliox inhalation therapy improves airway ventilation (Gluck et al., 1990), and decrease airway acidosis (Kass et al., 1995). A wide range of clinical measurement has been conducted for the acute asthma patient, and the heliox inhalation therapy is found more efficient for heliox based nebulization than air-driven nebulization (Bag et al., 2002; Kress et al., 2002; Lee et al., 2005; Sattonnet et al., 2004). Apart from the all positive findings, some clinical measurement are found less or no beneficial for the heliox-driven nebulization for adult asthma patient (Dorfman et al., 2000; Henderson et al., 1999; Rivera et al., 2006). However, their study is performed for a specific subject of disease and not applicable for all asthma patient. Almost all of the heliox based study only consider fluid flow in the extra- thoracic airways. The first particle based inhalation therapy reports heliox mixture is more efficient than air (Anderson et al., 1993). Later, nebulized aerosol therapy for obstructive child airway demonstrate that heliox improve the efficiency of the radio-aerosol transport to the distal alveoli (Piva et al., 2002). Recently, a numerical study for CT-based upper airway model reports that heliox inhalation therapy is better than air inhalation (Islam et al., 2018a). The numerical study considered only the first three generations of the lung and the understanding of the particle transport to the lower airways during heliox breathing is still unknown. The heliox inhalation therapy for a whole lung model is essential for better understanding of the heliox inhalation. This study aims to develop an advanced modelling framework for heliox breathing for a large-scale airway model.

2. Numerical Methods

The present large-scale digital reference model developed by Schmidt et al. (2004), which is derived from high-resolution computed tomography imaging of an *in vitro* preparation. The large-scale 17 generations model consists of 1453 bronchi and exhibits highly asymmetric branching pattern. The airway branching pattern is based on Horsfield order. Ansys meshing module is used to construct the unstructured tetrahedral mesh for the bifurcating airways. A fine inflation layer mesh is employed near the wall for complex flow fields. Desne tetrahedral elements are generated at the bifurcating airways. A proper mesh refinement test has been performed, and the final mesh contains about 34 millions of the computational cells. The detail of the mesh information and grid refinement can be found in the author's other study (Islam et al., 2018b; Islam et al., 2017a; Islam et al., 2017b). ANSYS 19 solver is used for the overall calculations. Euler-Lagrangian based Discrete Phase Model (Islam et al., 2017c)(DPM), and species transport model are considered to calculate the microparticle transport and deposition in the upper airways. The air is considered as the primary phase, and the particle is the secondary phase in DPM. The equation for conservation of mass can be written as follows:

$$\frac{\partial \rho}{\partial t} + \nabla.(\rho \vec{v}) = S_m \tag{1}$$

The source S_m is the mass added to the continuous phase from the dispersed second phase and any user-defined sources. The conservation of momentum in an inertial (non-accelerating) reference frame is described by;

$$\frac{\partial}{\partial t}(\rho \vec{v}) + \nabla.(\rho \vec{v}\vec{v}) = -\nabla p + \nabla.\left(\mu\left[(\nabla \vec{v} + \nabla \vec{v}^T) - \frac{2}{3}\nabla.\vec{v}I\right]\right) + \rho\vec{g} + \vec{F} \tag{2}$$

where p is fluid static pressure, $\rho\vec{g}$ is body force due to gravity, and $\vec{F}$ is body force due to external (particle-fluid interaction) force. The stress tensor is associated with the molecular viscosity (μ) and the unit tensor (I).

The chosen k-ω model is based on the Wilcox (1998), which incorporates modification of compressibility, low-Reynolds number effects and shear flow spreading. This is also based on model transport equations for turbulence kinetic energy (k) and the specific dissipation rate (ω).

Turbulence kinetic energy and specific dissipation rates are obtained from the following transport equations:

$$\frac{\partial}{\partial t}(\rho k) + \frac{\partial}{\partial x_i}(\rho k u_i) = \frac{\partial}{\partial x_j}\left(\Gamma_k \frac{\partial k}{\partial x_j}\right) + G_k - Y_k + S_k \tag{3}$$

And

$$\frac{\partial}{\partial t}(\rho \omega) + \frac{\partial}{\partial x_i}(\rho \omega u_i) = \frac{\partial}{\partial x_j}\left(\Gamma_\omega \frac{\partial \omega}{\partial x_j}\right) + G_\omega - Y_\omega + S_\omega \tag{4}$$

where G_k is the turbulence kinetic energy due to mean velocity gradients, G_ω is the generation of ω . Γ_k and Γ_ω are the effective diffusivity of k and ω, respectively. Y_k and Y_ω represent the dissipation of k and ω due to turbulence respectively. S_k and S_ω are source terms.

The effective diffusivities for the k-ω model are given by

$$\Gamma_k = \mu + \frac{\mu_t}{\sigma_k} \tag{5}$$

$$\Gamma_\omega = \mu + \frac{\mu_t}{\sigma_\omega} \tag{6}$$

where σ_k and σ_ω are turbulent Prandtl numbers, and μ_t is turbulent viscosity defined by

$$\mu_t = \alpha^* \frac{\rho k}{\omega} \tag{7}$$

Low Reynolds correction is used for the k-ω option. The coefficient α^*, damps turbulent viscosity, causing a low Reynolds number correction, which is given by

$$\alpha^* = \alpha_\infty^* \left(\frac{\alpha_0^* + \frac{Re_t}{R_k}}{1 + \frac{Re_t}{R_k}}\right) \tag{8}$$

The species transport equation for i_{th} species

$$\frac{\partial}{\partial t}(\rho Y_i) + \nabla.(\rho \vec{v} Y_i) = -\nabla.\vec{J}_i + R_i + S_i \quad (9)$$

where the net rate of production of species *i* is R_i and S_i is the rate of creation by addition from the dispersed phase plus any user-defined sources. An equation of this form is solved for *n-1* species where *n* is the total number of fluid phase chemical species present in the system. Since the mass fraction of the species must sum to unity, the *n* th mass fraction is determined as one minus the sum of the *n-1* solved mass fractions. To minimize numerical error, the n_{th} species is selected as that species with the overall largest mass fraction.

The mass diffusion for the turbulent case is defined as;

$$\vec{J}_i = -\left(\rho D_{i,m} + \frac{\mu_t}{Sc_t}\right)\nabla Y_i - D_{T,i}\frac{\nabla T}{T} \quad (10)$$

where Sc_t is the turbulent Schmidt number.

The overall numerical investigation is performed for different physical activity conditions, and different diameter microparticles are considered. The aerosol particle density is considered as $1100\ kg/m^3$. For the heliox mixture model, 80% helium and 20% oxygen is used. The velocity inlet and pressure outlet boundary conditions are used for the present study (Islam et al., 2015). A total of 15000 particles are injected from the surface of the tracheal inlet. The stationary wall and no-slip shear condition are used. The wall DPM boundary condition is used as trap, and heat flux thermal condition is used at the wall. All of the particles are injected at once.

3. Results

The present numerical study analyzed the airflow and particle transport to the terminal bronchioles of a large-scale 17-generations model. The overall investigation is performed for heliox and air breathing. The numerical simulation is performed for 15 l/min and 60 l/min flow rates. The airflow and pressure distribution are analyzed during heliox and air breathing. The overall investigation is carried out for one-way inhalation, and monodisperse particles are considered for the present study.

Airflow contours at the tracheal region and the different lobes of the lung are investigated for heliox and air breathing. Figure 1 shows the velocity contours at different selected planes of the lung at 15 l/min flow rate. The velocity contour at different selected planes on five different lobes is found different for heliox and air breathing. At the tracheal region, the velocity contour shows a fully developed flow contour for heliox and air breathing. The velocity contour illustrates a lower velocity magnitude near the tracheal wall for heliox breathing than air breathing. The density of the heliox mixture (0.5g/l) is significantly lower than the air density (1.25 g/l). The lower density of the heliox mixture creates lower resistance for the airflow than air and reduces the turbulent fluctuation at the tracheal wall. The lower turbulent intensity and lower velocity magnitude near the airway wall for heliox breathing eventually reduce the deposition efficiency at the upper airways. The velocity contours at the RUL and RML lobes are found significantly different for heliox and air breathing. For air-breathing case, the vortex is generated at the RUL and RML at 15 l/min flow rate. The higher turbulent fluctuation, pressure-driven force and complex curvature of the bifurcating airways influence the flow pattern for highly dense air than less dense heliox mixture. The velocity contour at RUL and RML lobes also shows lower velocity magnitude near the airway wall for heliox breathing than air. The velocity contours at the LUL and RUL show a similar velocity distribution at 15 l/min flow rate. The overall velocity contour for the LUL and LLL for heliox breathing is found different than air breathing.

The pressure contour for the 17-generations model at different flow rates is investigated. Figure 2 shows the pressure contour comparison for heliox and air breathing. Figures 2(a, b) show the pressure contour for heliox and air-breathing, respectively. The overall pressure magnitude shows higher pressure at the upper airways for air-breathing than heliox breathing. The higher pressure at the upper airways indicates higher airway resistance for air breathing. The maximum calculated pressure for air-breathing is slightly higher than heliox breathing. Figures 2(c, d) show the pressure contour for heliox and air-breathing at 60 l/min flow rate, respectively. The maximum pressure for air-breathing is found significantly higher than air breathing at 60 l/min flow rate. Figure 2(e) shows the pressure drop at RLL for heliox and air breathing.

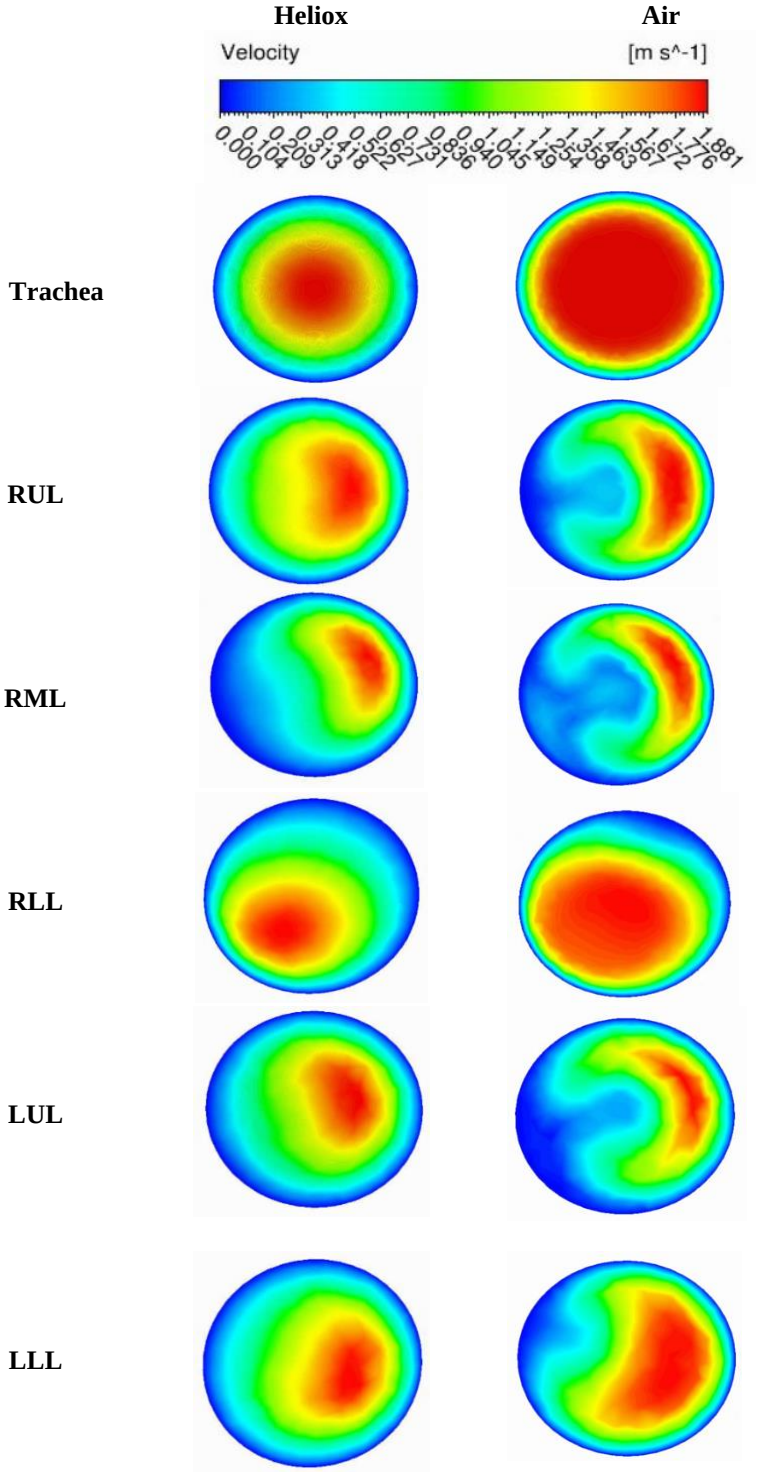

Fig. 1: Velocity contour at the selected planes of the 17-generation model for heliox and air-breathing (RUL= right upper lobe, RML= right middle lobe, LLL = right lower lobe, LUL = left upper lobe and LLL =left lower lobe) at 15 l/min flow rate.

The aerosol particle transport to the terminal airways of the 17-generations model has been investigated. Figure 3 shows the deposition pattern of 5-μm diameter aerosol particle for air and heliox breathing. Figure 3(a) shows the deposition pattern for air-breathing, and figure 3(b) shows the deposition pattern for heliox breathing. The overall deposition pattern shows more aerosol particle deposition for air-breathing than heliox breathing. The general deposition scenario of 5-μm diameter particle reports that a higher number of particles are deposited at the upper

airways for air-breathing than heliox breathing. The higher density of the air influences the overall deposition pattern during air breathing. The calculated velocity contour in figure 1 also supports the deposition pattern of figure 3. For air-breathing, the velocity magnitude near the airway wall is found higher than heliox breathing, and the higher near-wall velocity magnitude influences the deposition pattern.

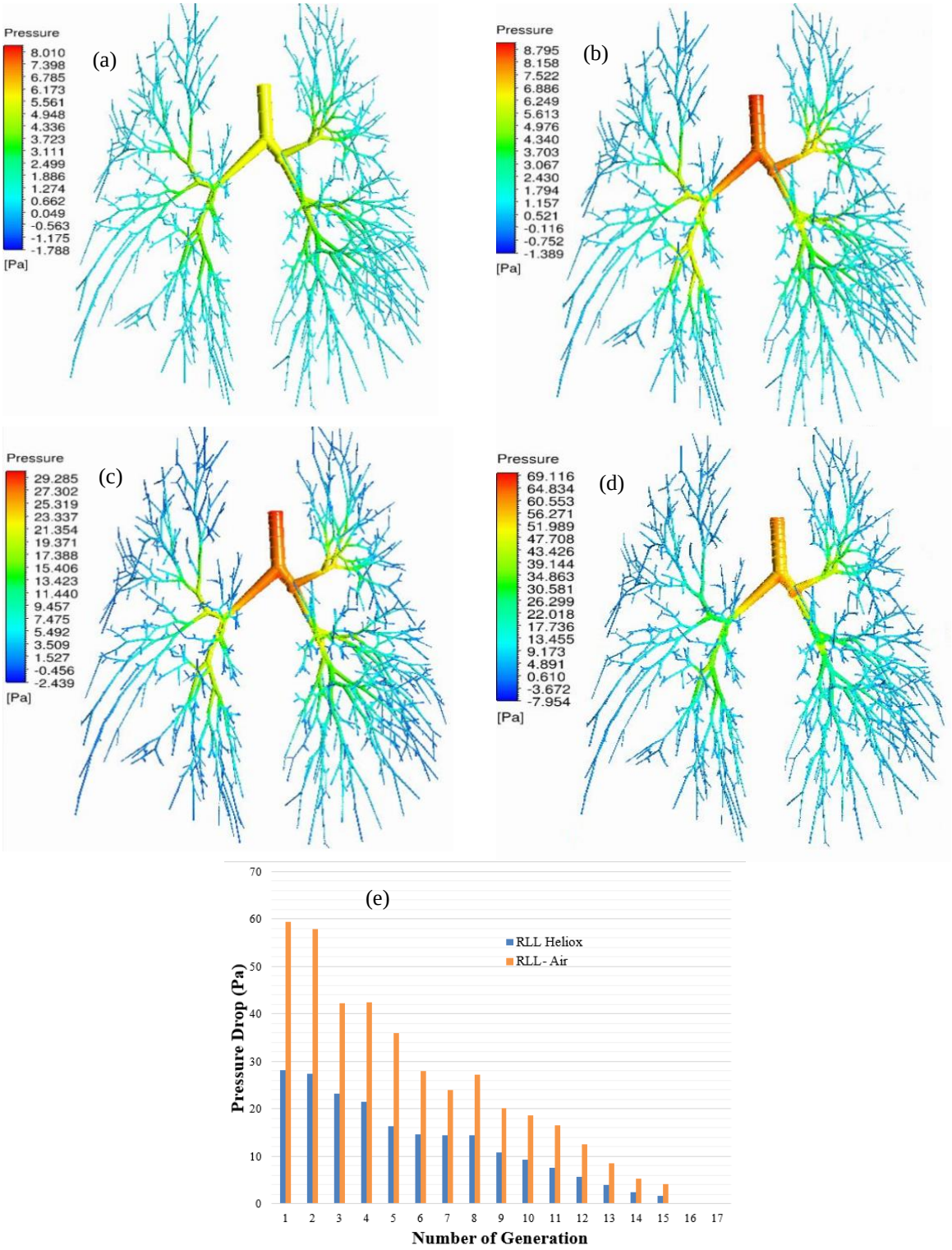

Fig. 2: The pressure distribution for 17-generations model at different flow rates, (a) heliox-15 l/min, (b) air-15 l/min, (c) heliox-60 l/min, (d) air-60 l/min and (e) pressure drop at 60 l/min.

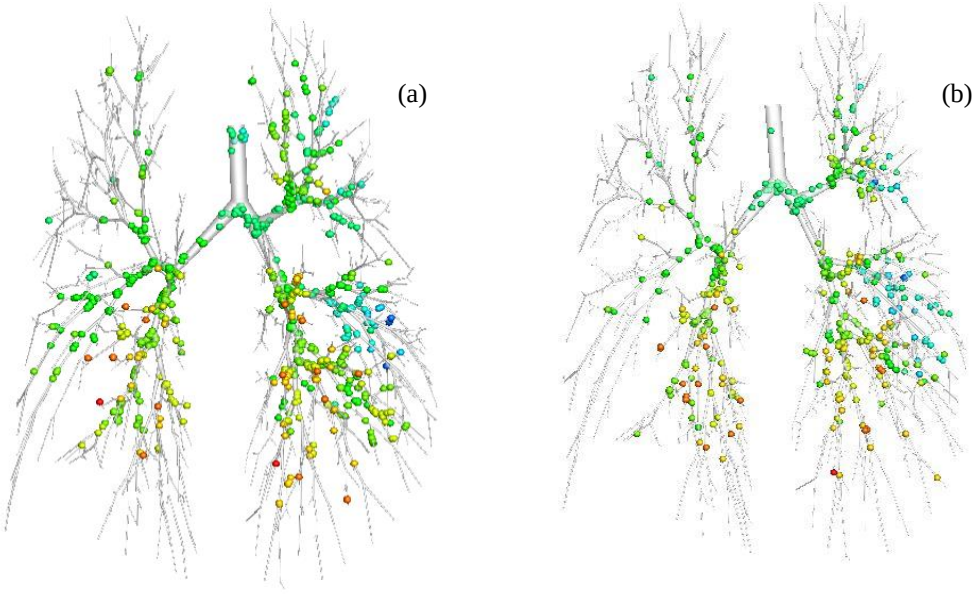

Fig. 3: Aerosol particle deposition pattern in a 17-generation lung model, (a) 60 l/min flow rate- Air and (b) 60 l/min flow rate- Heliox.

4. Conclusions

This study investigates aerosol particle transport and deposition to the terminal bronchioles for heliox breathing. The airflow and particle transport comparison is performed for different flow rates. Air and helium-oxygen breathing are considered for the present study. The numerical study calculated deposition pattern for different flow rates. The major conclusions from the present study are listed below:

- The velocity magnitude near the airway wall for heliox breathing is lower than the air breathing.
- The calculated pressure at the upper airways for air-breathing is higher than the heliox breathing at 15 l/min flow rate. At 60 l/min flow rate, the maximum pressure for air-breathing is found 2.36 times higher than heliox breathing.
- The overall deposition is found higher for air-breathing than heliox breathing.

The findings of the present study, along with more case-specific study, will increase the knowledge of the filed. A comprehensive patient-specific mixture model will be considered in the future.

Acknowledgments

The authors would like to acknowledge the computing facility of UTS Tech Lab. The authors also would like to thank Dr Tevfik Gemci for providing the geometry data.

References

Anderson, M., Svartengren, M., Bylin, G., Philipson, K., Camner, P., 1993. Deposition in asthmatics of particles inhaled in air or in helium-oxygen. American Journal of Respiratory and Critical Care Medicine 147, 524-528.

Bag, R., Bandi, V., Fromm Jr, R.E., Guntupalli, K.K., 2002. The effect of heliox-driven bronchodilator aerosol therapy on pulmonary function tests in patients with asthma. Journal of Asthma 39, 659-665.

Barach, A.L., 1935. The use of helium in the treatment of asthma and obstructive lesions in the larynx and trachea. Annals of Internal Medicine 9, 739-765.

Dorfman, T.A., Shipley, E.R., Burton, J.H., Jones, P., Mette, S.A., 2000. Inhaled heliox does not benefit ED patients withmoderate to severe asthma. The American journal of emergency medicine 18, 495-497.

Gluck, E.H., Onorato, D.J., Castriotta, R., 1990. Helium-oxygen mixtures in intubated patients with status asthmaticus and respiratory acidosis. Chest 98, 693-698.

Henderson, S.O., Acharya, P., Kilaghbian, T., Perez, J., Korn, C.S., Chan, L.S., 1999. Use of heliox-driven nebulizer therapy in the treatment of acute asthma. Annals of emergency medicine 33, 141-146.

https://lungfoundation.com.au/health-professionals/clinical-resources/copd/copd-the-statistics/.

Islam, S. C. Saha, Young, P.M., 2018a. Aerosol Particle Transport and Deposition in a CT-Based Lung Airway for Helium-Oxygen Mixture. 21st Australasian Fluid Mechanics Conference, Adelaide, Australia.

Islam, M.S., Saha, S.C., Gemci, T., Yang, I.A., Sauret, E., Gu, Y.T., 2018b. Polydisperse Microparticle Transport and Deposition to the Terminal Bronchioles in a Heterogeneous Vasculature Tree. Scientific Reports 8, 16387.

Islam, M.S., Saha, S.C., Sauret, E., Gemci, T., Gu, Y., 2017a. Pulmonary aerosol transport and deposition analysis in upper 17 generations of the human respiratory tract. Journal of Aerosol Science 108, 29-43.

Islam, M.S., Saha, S.C., Sauret, E., Gemci, T., Yang, I.A., Gu, Y., 2017b. Ultrafine Particle Transport and Deposition in a Large Scale 17-Generation Lung Model. Journal of Biomechanics.

Islam, M.S., Saha, S.C., Sauret, E., Gu, Y., Molla, M.M., Year Numerical investigation of diesel exhaust particle transport and deposition in the CT-scan based lung airway. In AIP Conference Proceedings.

Islam, M.S., Saha, S.C., Sauret, E., Gu, Y., Ristovski, Z., Year Numerical investigation of aerosol particle transport and deposition in realistic lung airway. In Proceedings of the International Conference on Computational Methods.

Kass, J.E., Castriotta, R.J., 1995. Heliox therapy in acute severe asthma. Chest 107, 757-760.

Kim, I.K., Corcoran, T., 2009. Recent developments in heliox therapy for asthma and bronchiolitis. Clinical Pediatric Emergency Medicine 10, 68-74.

Kress, J.P., Noth, I., Gehlbach, B.K., Barman, N., Pohlman, A.S., Miller, A., Morgan, S., Hall, J.B., 2002. The utility of albuterol nebulized with heliox during acute asthma exacerbations. American journal of respiratory and critical care medicine 165, 1317-1321.

Lee, D.L., Hsu, C.W., Lee, H., Chang, H.W., Huang, Y.C.T., 2005. Beneficial effects of albuterol therapy driven by heliox versus by oxygen in severe asthma exacerbation. Academic emergency medicine 12, 820-827.

Piva, J.P., Barreto, S.S.M., Zelmanovitz, F., Amantéa, S., Cox, P., 2002. Heliox versus oxygen for nebulized aerosol therapy in children with lower airway obstruction. Pediatric Critical Care Medicine 3, 6-10.

Reuben, A., Harris, A., 2004. Heliox for asthma in the emergency department: a review of the literature. Emergency Medicine Journal 21, 131-135.

Rivera, M.L., Kim, T.Y., Stewart, G.M., Minasyan, L., Brown, L., 2006. Albuterol nebulized in heliox in the initial ED treatment of pediatric asthma: a blinded, randomized controlled trial. The American journal of emergency medicine 24, 38-42.

Rodrigo, G., Rodrigo, C., Pollack, C., Travers, A., 2001. Helium-oxygen mixture for nonintubated acute asthma patients. The Cochrane database of systematic reviews, CD002884-CD002884.

Sattonnet, P., Plaisance, P., Lecourt, L., Vicaut, E., Adnet, F., Goldstein, P., Chollet, C., Marx, J., Ecollan, P., Lambert, Y., 2004. The efficacy of helium-oxygen mixture (65%–35%) in acute asthma exacerbations. Emergency Medicine Australasia 16, A71.

Schmidt, A., Zidowitz, S., Kriete, A., Denhard, T., Krass, S., Peitgen, H.-O., 2004. A digital reference model of the human bronchial tree. Computerized Medical Imaging and Graphics 28, 203-211.

Skloot, G.S., 2017. The effects of aging on lung structure and function. Clinics in geriatric medicine 33, 447-457.

Valli, G., Paoletti, P., Savi, D., Martolini, D., Palange, P., 2007. Clinical use of Heliox in asthma and COPD. Monaldi archives for chest disease 67.

Wilcox, D.C., 1998. Turbulence modeling for CFD. DCW industries La Canada, CA.